Research Paper

A circadian rhythm-related gene signature associated with tumor immunity, cisplatin efficacy, and prognosis in bladder cancer

Ranran Zhou[1,2], Xinyu Chen[1,2], Jingjing Liang[3], Qi Chen[1,2], Hu Tian[1,2], Cheng Yang[1,2], Cundong Liu[1,2]

[1]Department of Urology, The Third Affiliated Hospital of Southern Medical University, Guangzhou, China
[2]The Third School of Clinical Medicine, Southern Medical University, Guangzhou, China
[3]Department of Cardiology, Shunde Hospital of Southern Medical University, Foshan, China

Correspondence to: Cundong Liu; **email:** Cundongliu@163.com, https://orcid.org/0000-0002-2098-1139

ABSTRACT

Circadian dysregulation involves malignant tumor initiation and progression, but the understanding of circadian rhythm's roles in bladder cancer (BCa) remains insufficient. The circadian rhythm-related genes were collected and clustered based on the Cancer Genome Atlas (TCGA), and the clustering was significantly associated with the prognosis and risk clinicopathological features. Through genomic difference analysis and gene pairing, a circadian rhythm-related signature was successfully established. Kaplan-Meier survival analysis and time-dependent receiver operating curves displayed that the prognosis model was a reliable prognosis biomarker both in the training cohort (n = 396, P = 2.687e-10) and external validation cohort (n = 224, P = 1.45e-02). The patients with high risk have high immune infiltration and high expression of immune checkpoint genes, which partly account for the poor prognosis. TIDE algorithm and the validation in IMvigor210 cohort indicated that the risk signature was a promising marker for the immunotherapeutic response. The risk model could also predict the therapeutic response of cisplatin, which was validated in the Genomics of Drug Sensitivity in Cancer database (P = 0.0049), TCGA (P = 0.038), and T24 BCa cells treated with cisplatin. The functional enrichment showed the risk model was significantly correlated with some malignant phenotypes, such as angiogenesis, epithelial-mesenchymal transition, and KRAS signaling pathway. Totally, we proposed a novel circadian rhythm-related signature for prognosis evaluation, which also helped to predict the immune infiltration and cisplatin sensitivity in BCa.

INTRODUCTION

Bladder cancer (BCa), one of the leading causes of human death worldwide, carries high morbidity and mortality. The inconspicuous early symptoms make a large number of patients have local metastasis when they are clinically diagnosed [1]. Despite the considerable progress made in medical therapy, such as cisplatin-based neoadjuvant chemotherapy and immune checkpoint inhibitors (ICIs), the 5-year survival rate of muscle-invasive bladder cancer (MIBC) is dismal 5%-20% [2]. Therefore, precise and

reliable prognosis prediction is always a hot topic in the field of BCa.

With the development of gene sequencing and big-data analysis, some gene-based models associated with BCa prognosis have been proposed [3, 4]. The established models were always based on some biological functions or processes, such as ferroptosis [5], hypoxia [6], and smoking [7], providing useful clinical tools and cut-in points to investigate the mechanisms. Nevertheless, seeking more accurate predictions remains essential and meaningful.

Circadian rhythm is a phenomenon in the life activities of the body, such as physiology, biochemistry and behaviour, which are periodically driven by the clock genes and clock-control genes, and the period is approximately 24 hours [8]. The circadian rhythm plays an essential role in maintaining homeostasis. Epidemiological studies have found that circadian disorders caused by shift work may increase the risk of cancer [9]. The relationships between malignant tumors and circadian rhythm receive more and more attention [10, 11]. However, few studies focus on circadian rhythm functions in BCa for the moment, and further researches are urgently demanded.

Here, we identified circadian rhythm as a prognostic factor for BCa prognosis via unsupervised clustering and screened multiple biomarkers to construct a circadian rhythm-related signature to evaluate overall survival (OS). To achieve a widespread utility, we adopted a gene-pair strategy for the model establishment, and there is no need for a definite gene expression value [12]. The predictive value of the established model was validated in different independent cohorts. Besides, the associations of the risk signature with tumor immune infiltration and immunotherapeutic response were explored. The predictive value to cisplatin effectiveness was also detected through multi-database analyses and vitro experiments.

RESULTS

Circadian rhythm was associated with prognosis in BCa

The circadian rhythm-related genes were retrieved from the Molecular Signatures Database (MSigDB, https://www.gsea-msigdb.org/gsea/msigdb/), as displayed in Supplementary Table 1. A sum of 290 circadian-related genes was extracted after excluding the overlapped genes. Accordingly, the Cancer Genome Atlas (TCGA) cases were clustered into two subgroups, containing Cluster A and B, via unsupervised clustering (Figure 1A–1C and Supplementary Table 2). The patients in Cluster A exhibited worse OS compared with those in Cluster B ($P < 0.01$, Figure 1D), and more deaths were observed in Cluster A ($P < 0.01$, Figure 1E). Besides, the circadian clustering was also significantly associated with the risk clinicopathological features, such as tumor grade ($P < 0.001$, Figure 1H), pathological T stages ($P < 0.001$, Figure 1I), and tumor stages ($P < 0.001$, Figure 1L), while gender (Figure 1F), age (Figure 1G), pathological N stages (Figure 1J), and M stages (Figure 1K) showed statistical non-significance. These analyses suggested that the critical role circadian rhythm played in BCa might be underestimated, and further exploration was demanded given the previous poor reports.

Development of a circadian rhythm-related gene signature

The flow chart of the risk model construction is displayed in Figure 2A. The circadian genes with significant expression differences were chosen for further analysis, and 122 differentially-expressed genes (DEGs) between normal and BCa tissues were screened (Supplementary Table 3 and Figure 2B). Afterwards, 122 genes were cyclically paired, and 1667 gene pairs were established based on the gene-pair strategy [13], among which 38 pairs were associated with OS employing Lasso regression (Figure 2C, 2D). Univariate Cox analysis indicated 10 of the 38 genes pairs carried significant prognostic value with $P < 0.001$ filterings (Supplementary Table 4 and Figure 2E), and 8 of 10 pairs were ultimately included in the prognostic model through multivariate Cox analysis with stepwise (Supplementary Table 5). To help clinicians better understand the risk model, we drew a forest plot (Figure 2F) and a nomogram (Figure 2G). Here, the risk evaluated by the established model of each case was defined as the circadian rhythm-related score (CRRS). The CRRS was calculated as follows: 0.314*(PPP2CB|CRTC2) – 0.547*(PSMA4|NAMPT) + 0.330*(QKI|RBPMS) + 0.316*(ADA|MAPK10) – 0.688*(ARNT2|OPRL1) – 0.437*(ID2|SREBF1) – 0.559*(OGT|MEF2D) – 0.350*(TH|FBXL22), where (gene A| gene B) represented a gene pair. The value of this pair would be considered as 1 if the expression of gene A is higher than that of gene B; otherwise, it would be defined as 0. Subsequently, we conducted the functional enrichment of the high-CRRS patients via GSEA software (version. 4.1.0) and the reference gene sets associated with circadian rhythm were downloaded from MSigDB (Supplementary Table 1). Gene Set Enrichment Analysis (GSEA) showed circadian clock pathway was significantly enriched in the cases with high CRRS (Nominal $P < 0.05$, Figure 2H). The expression association between the 16 genes, which comprised the CRRS, and four known circadian transcription factors, including CLOCK, ARNTL, PER1, and PER2, were displayed in Supplementary Table 6 and Figure 2I, and most of the 16 genes exhibited significant correlation. The Sankey diagram showed the distribution of the patients in circadian clustering, CRRS estimation, and survival status (Figure 2J).

Validation of CRRS

Diverse methods were conducted to validate the robustness of the CRRS in different independent cohorts, including TCGA-BLCA and GSE32894. The baseline clinical traits of these two cohorts are shown in Table 1. According to the established formula, the risk of these patients was evaluated, and the optimal cut-off was equal to 0.313, which is the median CRRS in the training

dataset. The detailed information was supplemented in Supplementary Tables 7, 8. The 3- (Figure 3A) and 5-year (Figure 3B) Calibration plots indicated the predicted OS was similar to the ideal survival rates. Kaplan-Meier survival analyses showed the cases with high CRRS exhibited worse survival rates both in the TCGA-BLCA (P < 0.001, Figure 3C) and GSE32894 datasets (P < 0.05, Figure 3D). The receiver operating curves (ROC) of the 1-, 3-, and 5-year OS in the training dataset (Figure 3E) and external validation dataset (Figure 3F) verified the predictive value of the CRRS. Besides, more deaths were observed with the increasing CRRS (Figure 3G, 3H).

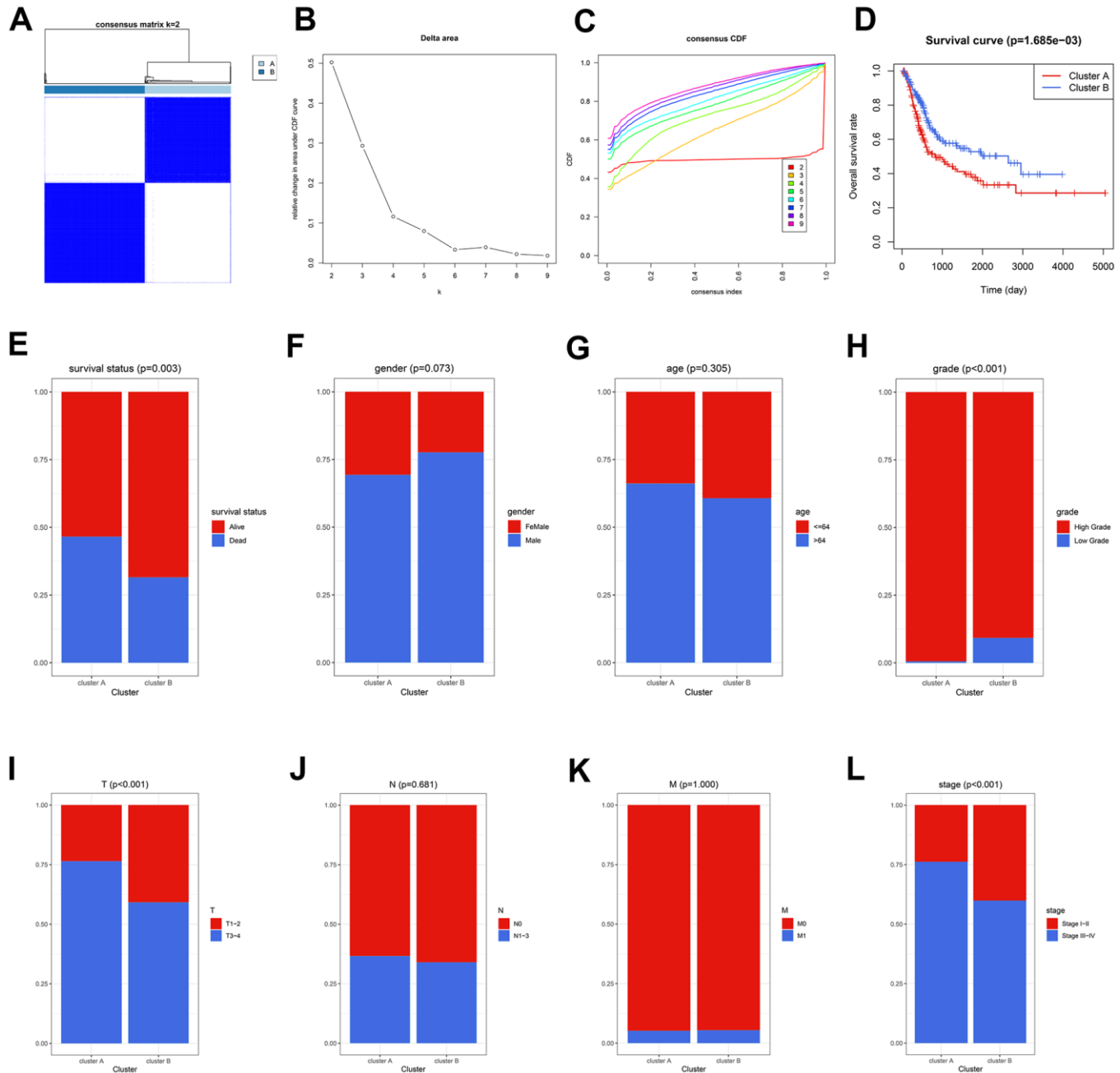To screen novel biomarkers, we compared the expression difference of these genes between adjacent normal and

Figure 1. The circadian rhythm was significantly associated with BCa prognosis. (**A**–**C**) The BCa patients were divided into two circadian subgroups via unsupervised clustering. (**D**) The Kaplan-Meier analysis displayed that the cases in Cluster A exhibited a worse prognosis. (**E**) More deaths were observed in Cluster A. (**F**–**L**) The association of circadian clustering with gender (**F**), age (**G**), grade (**H**), pathological T stages (**I**), pathological N stages (**J**), M stages (**K**), and tumor stages (**L**). BCa, bladder cancer.
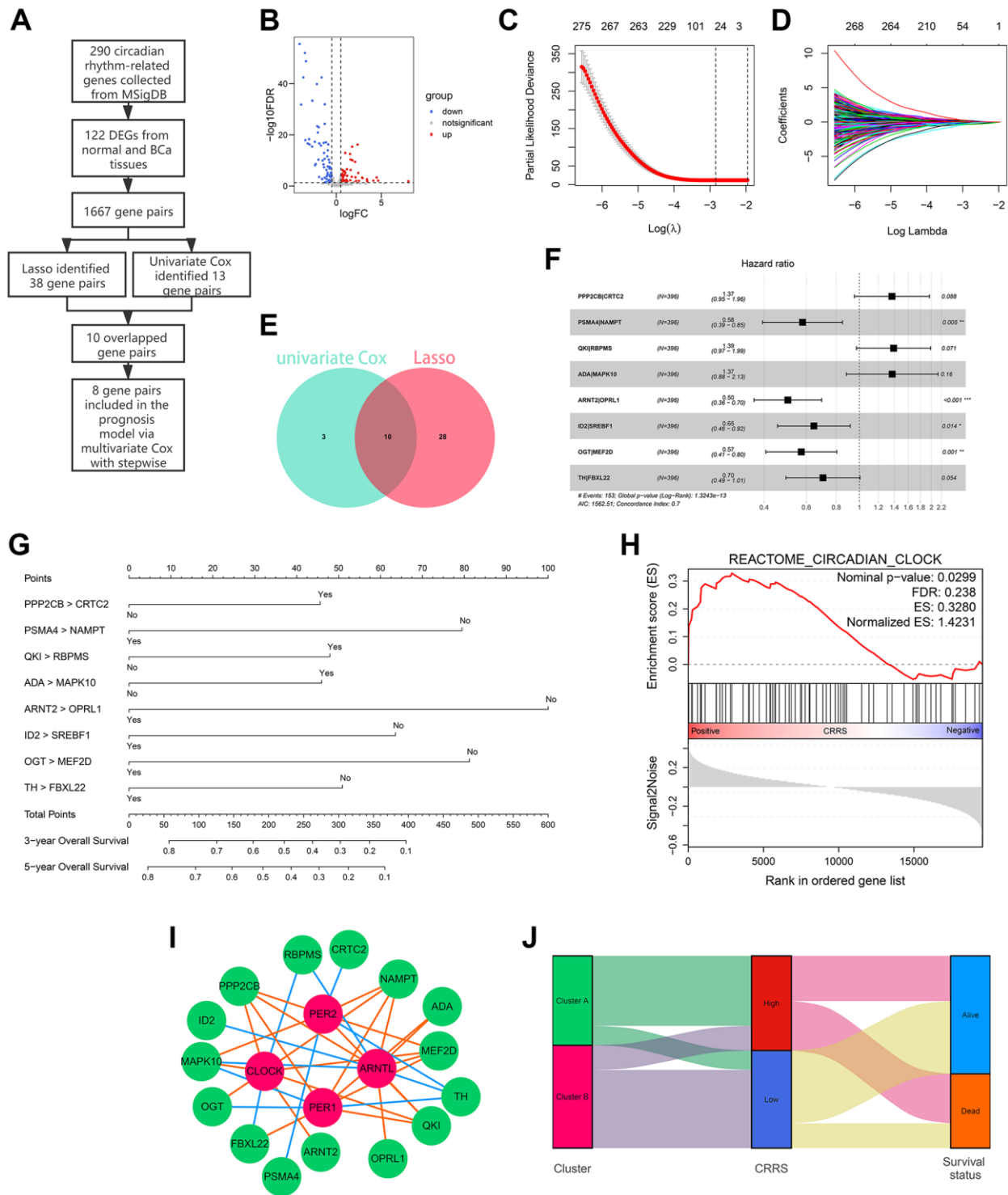
Figure 2. Development of a circadian rhythm-related signature. (**A**) The process of the prognostic model construction. (**B**) The volcano plot displaying 122 of 290 circadian rhythm-related genes were differentially expressed between adjacent normal and BCa tissues. (**C**, **D**) Lasso regression identified 38 gene pairs correlated with BCa prognosis. The lines with different colors represented different variables. (**E**) 10 gene pairs were con-determined via univariate Cox regression and Lasso algorithm. (**F**, **G**) The forest plot (**F**) and the nomogram (**G**) of the established model. (**H**) The circadian clock pathway was significantly up-regulated in patients with high CRRS. (**I**) The correlation between the genes in CRRS and known circadian transcription factors. The green bubbles and red bubbles represented the CRRS genes and transcription factors, respectively. The red lines and blue lines represented the positive and negative correlations, respectively. (**J**) The Sankey plot indicated the association between circadian clustering, CRRS stratification, and survival status. BCa, bladder cancer; CRRS, circadian rhythm-related score.

Table 1. The baseline information of 785 cases enrolled in the present study.

Parameters	TCGA (n=396)	GSE32894 (n=224)
Survival status		
Alive	243 (61.3%)	199 (88.8%)
Dead	153 (38.6%)	25 (11.1%)
Follow-up (day)	778.19 ± 814.38	1196.98 ± 767.38
Age	67.84 ± 10.53	69.43 ± 11.28
Gender		
Female	104 (26.2%)	61 (27.2%)
Male	292 (73.7%)	163 (72.7%)
Pathological Stage		
I	2 (0.5%)	-
II	124 (31.3%)	-
III	138 (34.8%)	-
IV	130 (32.8%)	-
Unknown	2 (0.5%)	-
pT stage		
T0	1 (0.2%)	0 (0.0%)
Ta	0 (0.0%)	110 (49.1%)
T1	3 (0.7%)	63 (28.1%)
T2	113 (28.5%)	43 (19.1%)
T3	190 (47.9%)	7 (3.1%)
T4	57 (14.3%)	1 (0.4%)
Unknown	32 (8.0%)	0 (0.0%)
M stage		
M0	189 (47.7%)	-
M1	10 (2.5%)	-
Unknown	197 (49.7%)	-
pN stage		
N0	229 (57.8%)	27 (12.0%)
N1	44 (11.1%)	3 (1.3%)
N2	75 (18.9%)	10 (4.4%)
N3	7 (1.7%)	0 (0.0%)
Unknown	41 (10.3%)	184 (82.1%)
Risk stratification		
High	195 (49.2%)	9 (4.0%)
Low	201 (50.7%)	212 (95.9%)
CRRS	0.41 ± 0.39	0.18 ± 0.081

TCGA, the Cancer Genome Atlas; CRRS, circadian rhythm-related score. The results are shown as mean ± standard deviation (SD).

BCa tissues utilizing the Wilcoxon signed-rank test (Supplementary Figure 1). In addition, the prognostic values of the 16 genes were also evaluated both in the TCGA-BLCA cohort (Supplementary Table 9 and Supplementary Figure 2) and the GSE32894 cohort (Supplementary Table 10 and Supplementary Figure 3), and X-tile was used to determine the optimal cut-off for Kaplan-Meier analyses [14]. The protein expression level of these genes between normal and BCa samples were also detected via immunohistochemistry (IHC), as supplemented in Supplementary Figure 4.

The clinical association of CRRS

As displayed in Figure 4A, CRRS was significantly correlated with age (P < 0.01), tumor grade (P < 0.001), tumor stage (P < 0.001), pathological T stages (P < 0.001), and M stages (P < 0.05) via Chi-square test after excluding the cases with unknown statuses.

Besides, the CRRS was superior to the clinicopathological features in OS prediction. The univariate (HR = 2.91, P < 0.01) and multivariate (HR = 2.83, P < 0.01)

analyses indicated that the CRRS was an independent risk factor after transforming the parameters into binary variables (Table 2). The areas under curve (AUCs) of each variable were calculated and compared. The predictive ability of the CRRS was better than other clinicopathological traits in 1- (AUC = 0.747, Figure 4B), 2- (AUC = 0.760, Figure 4C), 3- (AUC = 0.753, Figure 4D), 4- (AUC = 0.776, Figure 4E), and 5-year (AUC = 0.787, Figure 4F) ROC curves.
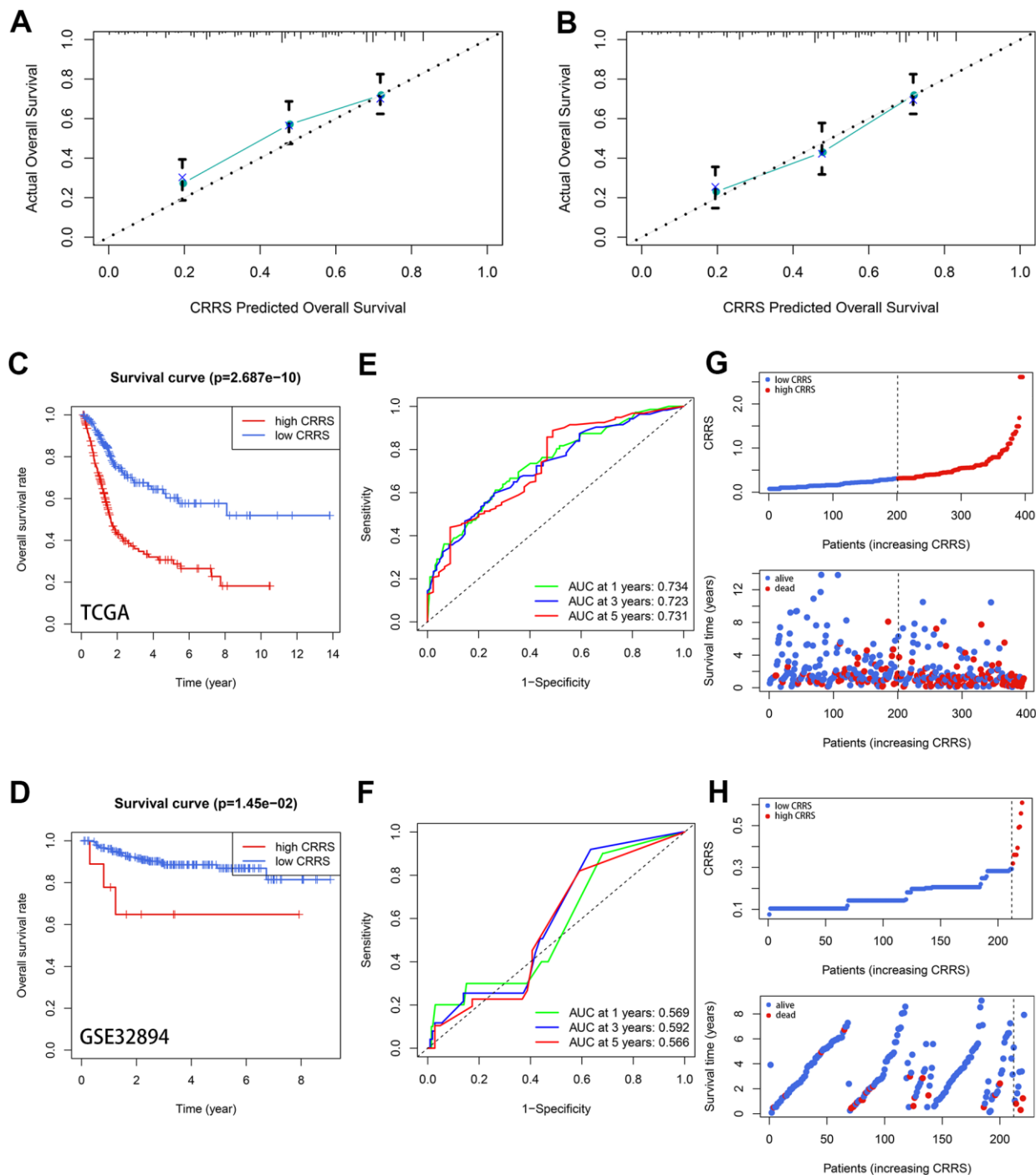

Figure 3. Validation of the prognostic value of CRRS. (**A**, **B**) The 3- (**A**) and 5-year (**B**) calibration plots. (**C**, **D**) The Kaplan-Meier survival analysis with a log-rank test in TCGA-BLCA cohort (**C**) and GSE32894 cohort (**D**). (**E**, **F**) The time-dependent ROC curve in TCGA-BLCA cases (**E**) and GSE32894 cases (**F**). (**G**, **H**) The distribution of the CRRS (up) and survival statuses (down) in the TCGA-BLCA cohort (**G**) and GSE32894 cohort (**H**). CRRS, circadian rhythm-related score; TCGA, the Cancer Genome Atlas; ROC, receiver operating curve.

The tumor immune infiltration profiles of CRRS

Seven clusters of immune and inflammatory genes were collected from previous studies, including lgG, HCK, MHC-II, LCK, MHC-I, STAT1, and interferon [15]. Gene Set Variation Analysis (GSVA) was conducted to quantify these immune and inflammatory responses (Supplementary Table 11). The heatmap (Figure 5A)
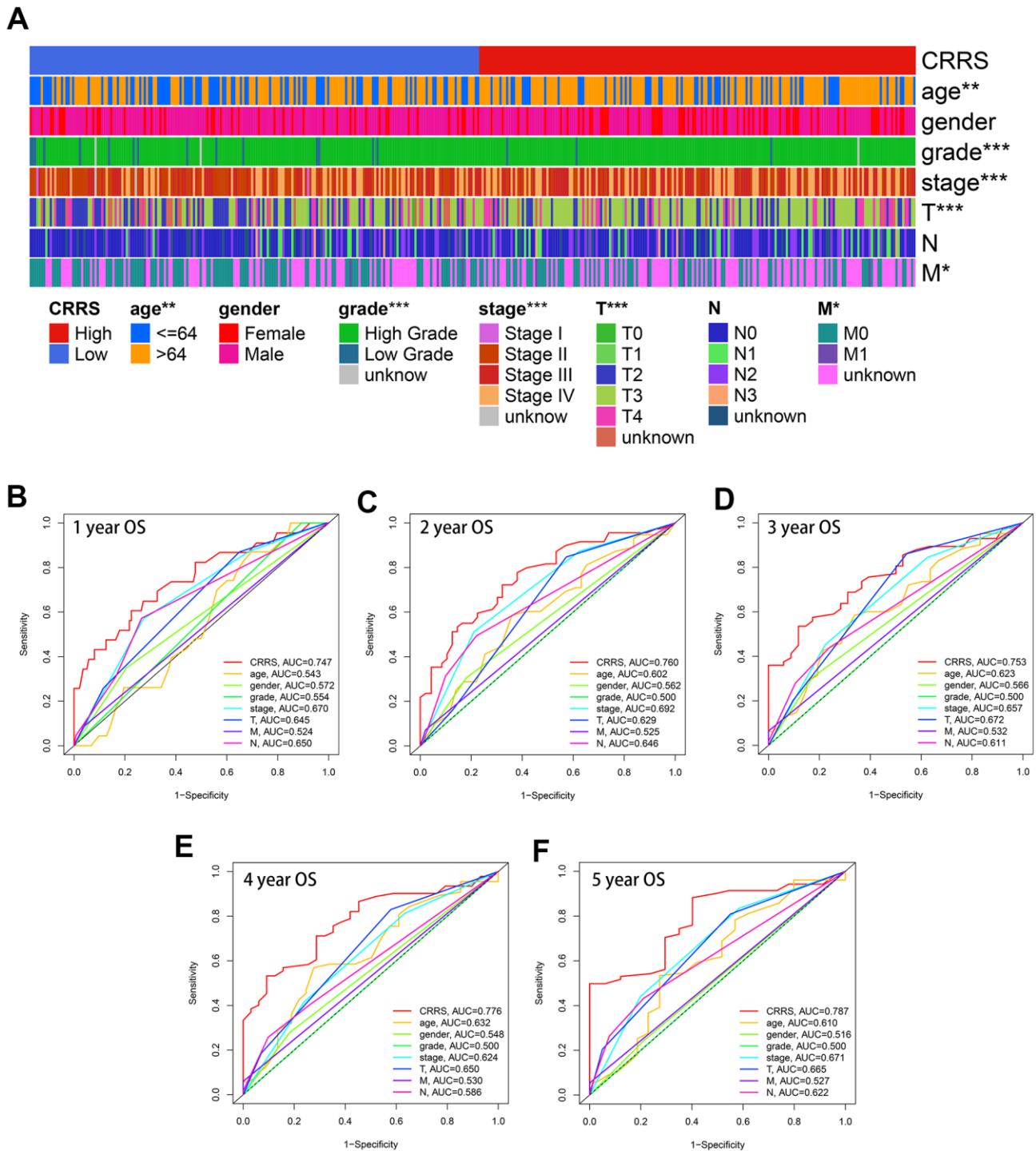

Figure 4. Clinical association of CRRS. (**A**) The heatmap indicating CRRS was significantly associated with age, gender, tumor grade, tumor stages, pathological T stages, and M stages utilizing Chi-square tests. (**B–F**). The time-dependent ROC analyses indicated the CRRS showed superiority over other clinical features in predicting the 1- (**B**), 2- (**C**), 3- (**D**), 4- (**E**), and 5-year (**F**) overall survival rate. ROC, receiver operating curve; CRRS, circadian rhythm-related score. *, P < 0.05; **, P < 0.01; ***, P < 0.001.

Table 2. Univariate and multivariate Cox analyses of CRRS.

Parameters	Univariate Cox		Multivariate Cox	
	HR (95%CI)	P value	HR (95%CI)	P value
Age (≤64 vs. >64)	1.42 (0.82-2.44)	0.204	1.32 (0.76-2.31)	0.322
Gender (Female vs. Male)	1.58 (0.94-2.66)	0.081	1.54 (0.91-2.61)	0.108
Grade (Low vs. High)	3.64 (0.50-26.53)	0.202	1.17 (0.15-9.30)	0.884
Stage (Stage I-II vs. Stage III-IV)	2.26 (1.15-4.44)	0.017	0.50 (0.15-1.67)	0.259
T (T 1-2 vs. T 3-4)	2.41 (1.26-4.61)	0.008	3.00 (0.99-9.13)	0.053
M (M0 vs. M1)	2.55 (1.02-6.40)	0.045	1.45 (0.54-3.87)	0.457
N (N0 vs. N1-3)	2.33 (1.45-3.78)	0.001	2.07 (1.19-3.63)	0.010
CRRS (Low vs. High)	2.45 (1.49-4.01)	< 0.001	2.32 (1.39-3.85)	0.001

HR, hazard ratio; CI, confidence interval; CRRS, circadian rhythm-related score.

and the boxplots (Figure 5B) showed the CRRS was positively associated with HCK, MHC-II, LCK, MHC-I, STAT1, and interferon. Intratumoral immune heterogeneity might account for the lack of association between CRRS and lgG. Besides, we also evaluated the immune activities with ESTIMATE [16], which was widely used for calculating the proportion of the stromal and immune components in the tumor microenvironment (TME), and the Wilcoxon test displayed the cases with high CRRS carried high tumor infiltration (Figure 5C). Subsequently, the infiltration of different immune cells, including B cells, CD4 T cells, CD8 T cells, neutrophils, macrophages, and dendritic cells, was estimated by the TIMER algorithm [17], and the significant positive association with the CRRS was found except for B cells (Figure 5D).

Given the high immune infiltration and unfavorable prognosis in the high-CRRS patients, we further explored the expression level of immune checkpoints and found that all the collected routine checkpoint genes exhibited significant expression differences (Figure 5E). The high expression level of the immune checkpoints might be responsible for the poor prognosis, implying that the cases with high CRRS were also sensitive to immunotherapy. Hence, some critical biomarkers indicating the immunotherapy efficacy, including CXCL9 [18], CXCL13 [18], and TIDE scores [19], were adopted to evaluate the immunotherapeutic sensitivity. Compared with the cases in the low-CRRS group, the patients in the high-CRRS group had higher expression levels of CXCL9 (P < 0.001) and CXCL13 (P < 0.001, Figure 5F). Th Chi-square test (P < 0.01, Figure 5G) displayed that the patients labelled with high CRRS would be more likely to benefit from the immunotherapy. CRRS could also serve as a prognosis biomarker for IMvigor210 cohort, who have received atezolizumab treatment (P < 0.05, Figure 5H). The calculated CRRSs of IMvigor210 cohort were shown in Supplementary Table 12.

The association between CRRS and cisplatin response

Based on the predicted half inhibitory concentration (IC50) of the patients from TCGA, we found the CRRS was significantly associated with the sensitivity of common chemotherapeutic agents, such as cisplatin (P < 0.001), doxorubicin (P < 0.01), gemcitabine (P < 0.001), methotrexate (P < 0.001), and vinblastine (P < 0.05, Figure 6A). Meanwhile, we downloaded the transcriptome expression values of 20 BCa cell lines and corresponding IC50 of the common chemotherapeutic drugs from Genomics of Drug Sensitivity in Cancer (GDSC, https://www.cancerrxgene.org/) database [20]. The CRRS of each cell line was evaluated, and the risk stratification was based on the median CRRS in the TCGA-BLCA cohort, which was mentioned above (Supplementary Table 13 and Figure 6B). We showed the cells with high CRRS exhibited a low IC50 of cisplatin (P < 0.01, Figure 6C), while no significance was achieved in doxorubicin (P > 0.05), gemcitabine (P > 0.05), methotrexate (P > 0.05), and vinblastine (P > 0.05, Supplementary Figure 5). The Spearman correlation analysis indicated the CRRS was tightly associated with the IC50 values (r = -0.58, P < 0.05, Figure 6D). The collected cisplatin response of TCGA-BLCA patients was also retrieved to serve as the clinical sample validation, and the cases reported to carry complete response to cisplatin have a significantly higher CRRS than the patients with stable disease (P < 0.05, Figure 6E).

Afterwards, the experimental validation was also conducted to verify the conclusion. We treated T24 cells with 20 µM cisplatin for 24 hours, which was reported in previous studies [21], to detect the expression difference of the 16 genes in the risk model. The real-time quantitative PCR (RT-qPCR) results were shown in Figure 6F, and the primers were supplemented in Supplementary Table 14. It was found that ADA (P < 0.001), CRTC2 (P < 0.001), ID2 (P < 0.05),
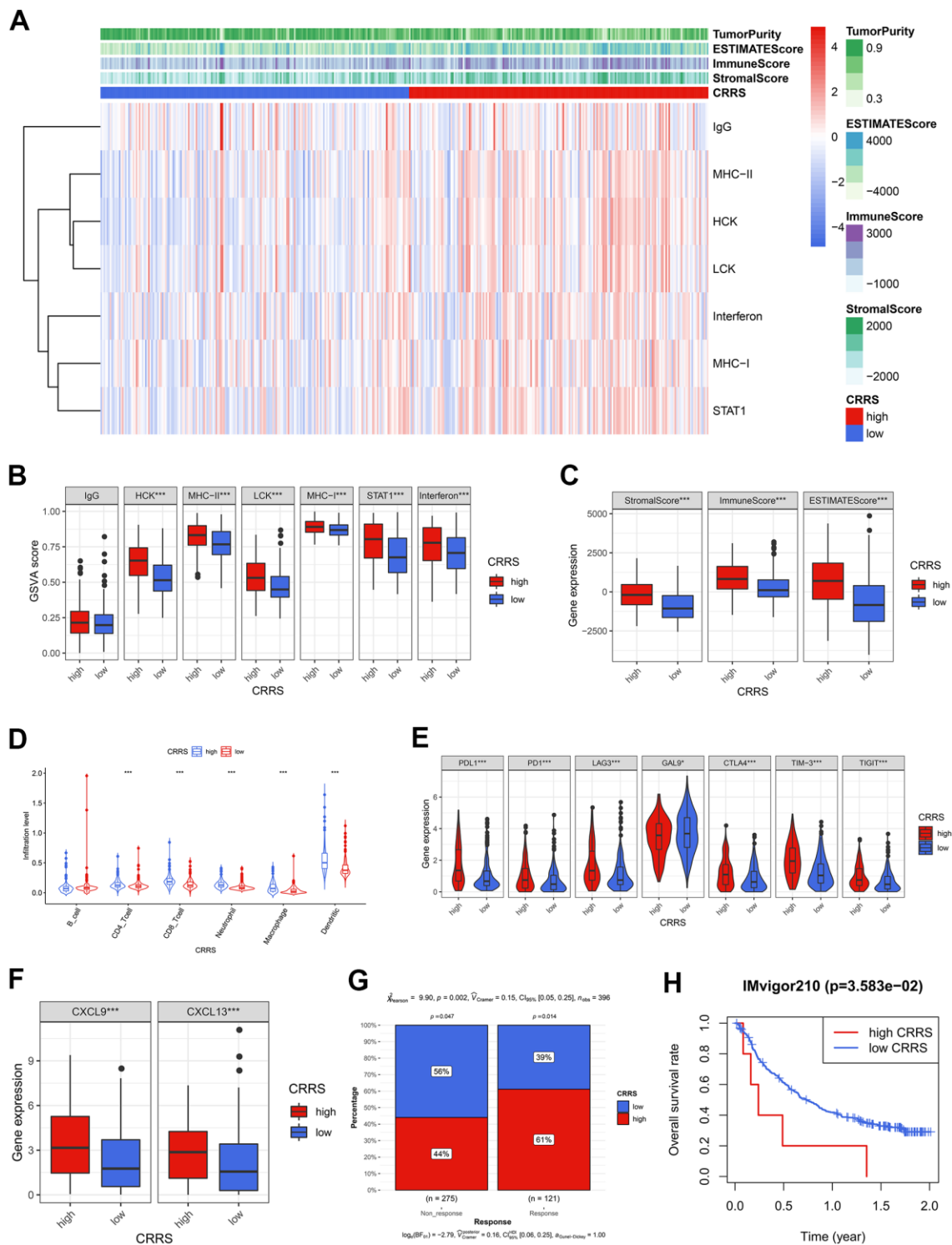
Figure 5. The tumor immune infiltration and CRRS. (**A**) The heatmap showed the GSVA scores of 7 immune and inflammatory gene clusters among the BCa patients with high and low CRRS. (**B**) 6 of 7 gene clusters were significantly associated with CRRS via Wilcoxon signed-rank tests. (**C**) The cases with high CRRS carried high Stromal Score, Immune Score, and ESTIMATE Score. (**D**) The patients in the high-CRRS group had a relatively higher infiltration proportion of CD4 T cells, CD8 T cells, neutrophils, macrophages, and dendritic cells. (**E**) The CRRS was positively associated with the expression of routine immune checkpoints, which included PD-L1, PD1, LAG3, GAL9, CTLA-4, TIM-3, and TIGIT. (**F**) The high expression of CXCL9 and CXCL13 was observed in the patients with high CRRS. (**G**) The Chi-square test indicated the high-CRRS patients were more likely to respond to immunotherapy. (**H**) CRRS was also a significant biomarker for prognosis in IMvigor 210 cohort. The optimal cut-off was determined by X-tile software. CRRS, circadian rhythm-related score; GSVA, gene set variation analysis; BCa, bladder cancer.
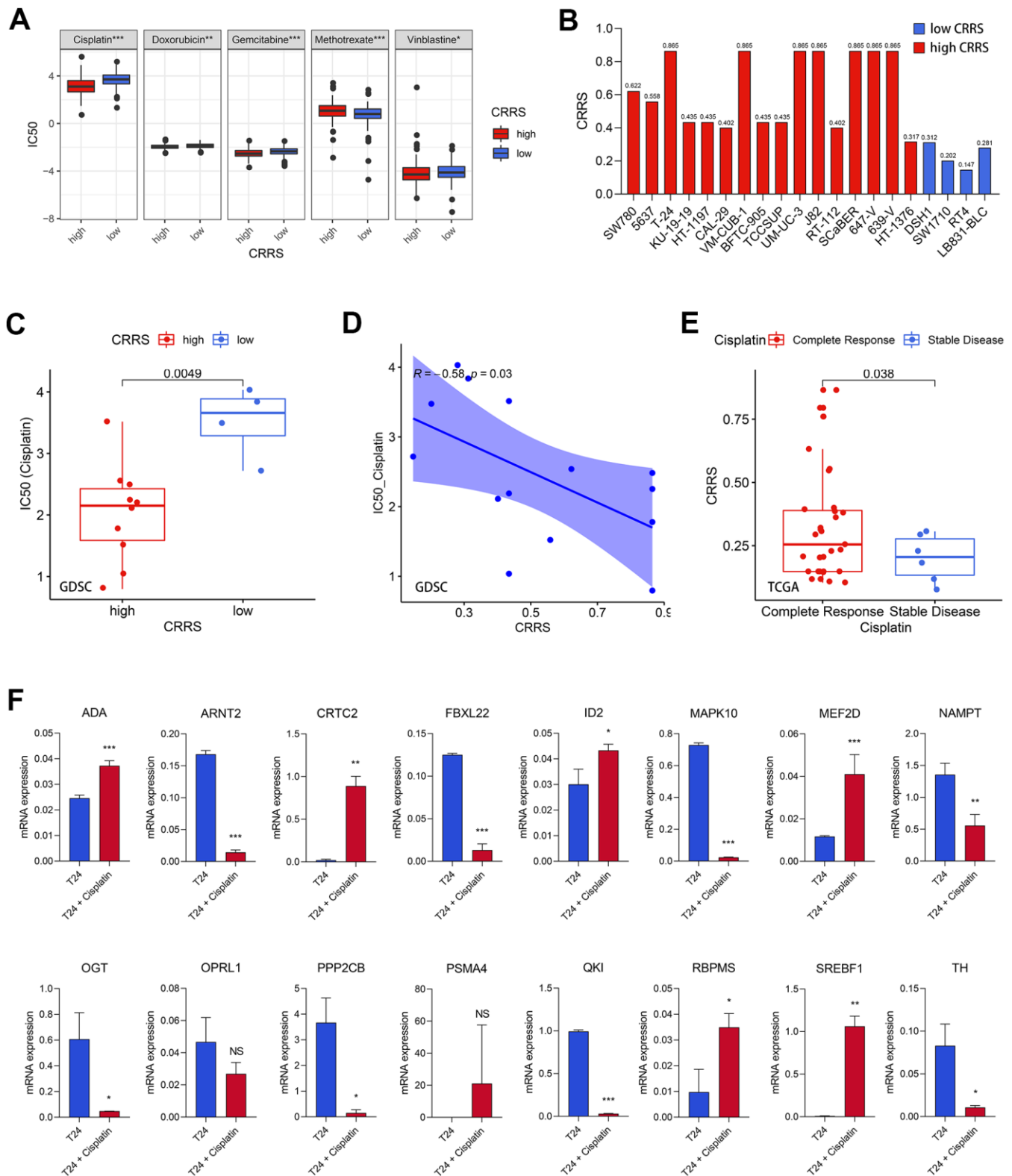
Figure 6. Cisplatin efficacy and CRRS. (**A**) The patients with high CRRS were more sensitive to cisplatin, doxorubicin, gemcitabine, and vinblastine, while the CRRS was positively associated with the sensitivity of methotrexate. (**B**) The evaluated CRRS and risk stratification of 20 BCa cell lines. (**C**) The cell lines with low CRRS exhibited high IC50 values via Wilcoxon signed-rank test. (**D**) The Spearman correlation analysis between CRRS and IC50 values among 20 BCa cell lines. (**E**) The patients with complete response had higher CRRS than those with stable disease. (**F**) The mRNA expression of the 16 CRRS genes after the treatment with 20μM cisplatin in T24 cells. CRRS, circadian rhythm-related score; IC50, half inhibitory concentration; BCa, bladder cancer.

MEF2D (P < 0.001), RBPMS (P < 0.05), and SREBF1 (P < 0.01) were significantly up-regulated in the T24 BCa cells treated with cisplatin, while ARNT2 (P < 0.001), FBXL22 (P < 0.001), MAPK10 (P < 0.001), NAMPT (P < 0.01), OGT (P < 0.05), PPP2CB (P < 0.05), QKI (P < 0.001), and TH (P < 0.05) were obviously decreased. Most of the 16 genes have significant expression differences after the treatment with cisplatin, re-validating the CRRS implicated cisplatin response.

Gene set variation analysis and gene set enrichment analysis

To detect the vital tumor phenotypes correlated with the CRRS, gene set enrichment analysis (GSEA) and GSVA were both performed. Through GSVA analysis, a sum of 9 hallmarks was identified, as shown in Supplementary Table 15 and Figure 7A, 7B. GSEA analysis screened 26 important tumor phenotypes, where the 9 hallmarks
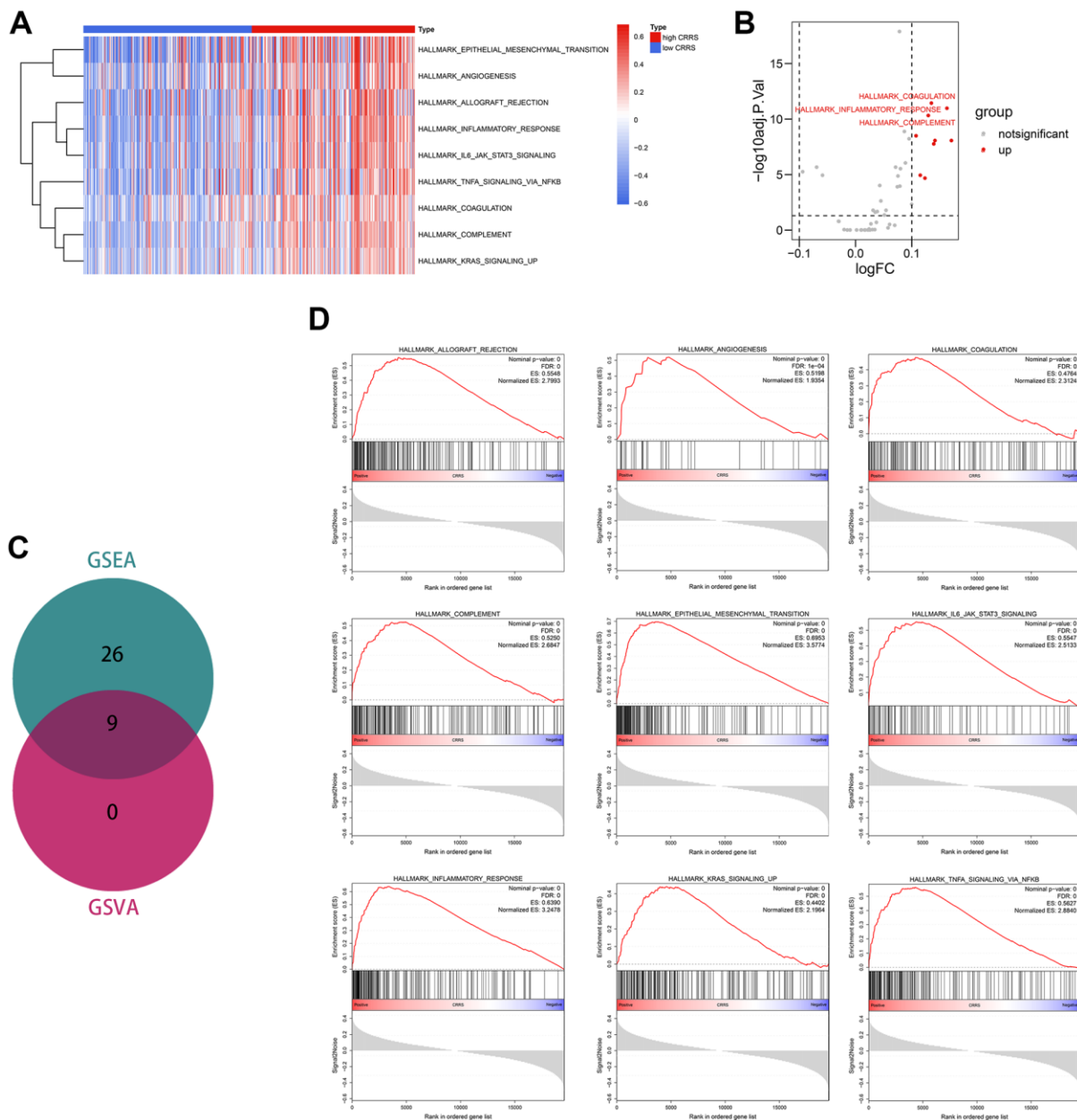

Figure 7. Functional enrichment analyses. (**A**) The heatmap displaying the significant phenotypes associated with CRRS. (**B**) A sum of 9 hallmarks was identified with the limma package. (**C**) Venn plot showing 9 phenotypes were overlapped from GSEA and GSVA analyses. (**D**) The overlapped 9 phenotypes included allograft rejection, angiogenesis, coagulation, complement, epithelial-mesenchymal transition, IL6-JAK-STAT3 signaling, inflammatory response, KRAS signaling, and TNFα signaling via NFKB. CRRS, circadian rhythm-related score; GSEA, gene set enrichment analysis; GSVA, gene set variation analysis.

were also included (Supplementary Tables 16, 17 and Figure 7C). The details of the 9 overlapped hallmarks are illustrated in Figure 7D.

DISCUSSION

At the molecular level, the circadian rhythm is formed by the oscillation of the clock gene to produce an autonomous rhythm. Circadian rhythm could regulate many biological processes, such as cell proliferation, cellular metabolism, and hormone secretion, which were the underlying mechanisms of circadian rhythm disorder in tumor initiation and progression [22]. Circadian rhythm dysregulation was often accompanied by the alternation of clock gene expression, which disrupted the normal cell cycle and thus directly promoted tumor cell proliferation [23, 24]. Melatonin, acting as a critical hormone regulating circadian rhythm, was significantly associated with the risk of breast cancer, lung cancer, and cervical carcinoma from previous evidence-based medical researches [25]. The findings above suggested circadian rhythm played an important role in tumori-genesis and tumor development. However, no circadian rhythm-related signature has been constructed in BCa, which is beneficial for personalized management and screening of new biomarkers.

The present study collected the circadian rhythm-related genes from MSigDB, and accordingly, 396 BCa patients were grouped into two clusters. We found the clustering was significantly associated with overall survival rate (P < 0.01) and many other risk clinical parameters, enlightening us to develop a circadian rhythm-related signature to identify significant biomarkers. To make the risk model widely appliable for the samples tested by RNA-seq, microarray, or RT-qPCR, a gene-pair strategy was adopted to construct the prognostic model based on the circadian rhythm-related genes which were differentially expressed between adjacent normal and BCa tissues. After Lasso and univariate Cox regression, a sum of 10 gene pairs was identified, 8 of which were included in the risk model via multivariate Cox regression with stepwise. According to the risk model, the risk of all BCa patients enrolled, including 396 cases from TCGA and 224 cases from GSE32894, was quantified as circadian rhythm-related score, or CRRS. CRRS was a promising predictive tool for BCa prognosis, which was validated in different independent cohorts. Besides, CRRS was superior to other clinico-pathological traits in OS evaluation.

The regulation of circadian rhythm to the immune system has been described [26–28]. The inflammation indicators in serum, such as TNF-α, IL-10, and C-reactive protein (CRP), were significantly increased in the subjects with circadian rhythm disorder [29].

Meanwhile, inflammatory factors could also influence the expression of core clock genes. Abreu et al. have found that the expression of BMAL1, PER2, and REV-ERB-α was obviously up-regulated in the Hodgkin lymphoma cells treated with TNF-α [30]. Previous researches suggested that circadian rhythm and immune system could influence each other. However, how circadian rhythm influenced the TME remains unclear. Here, we found the patients with high CRRS carried high immune infiltration and high checkpoint gene expression, which might account for the poor prognosis, and thus be more likely to benefit from immunotherapy. We screened some important biomarkers, which might be the cut-in points in future studies.

Cisplatin-based neoadjuvant chemotherapy remains one of the dominant medical treatments in BCa for the moment. Regarding how circadian rhythm affects cisplatin efficacy, several studies have been published. For instance, Wang et al. have found PER2, a circadian clock gene, enhanced the effect of cisplatin by suppressing PI3K/Akt pathway in ovarian cancer cells [31]. It was reported that circadian gene TIMELESS could decrease the cisplatin sensitivity by activating the Wnt/β-catenin pathway [32]. Besides, some researchers held that circadian rhythm was closely associated with DNA repair function and thus could influence cisplatin sensitivity since cisplatin serves as a DNA damaging agent [33]. Given the findings above, we explored the association between CRRS and cisplatin efficacy based on TCGA and GDSC databases and found CRRS was a promising clinical tool to evaluate the cisplatin response. The 16 genes, which comprised CRRS, mostly showed expression differences in T24 cells with cisplatin treatment. The results above re-validated the tight association between circadian rhythm and cisplatin and provided some important biomarkers.

Some genes comprising CRRS have been reported to involve the malignant phenotypes in different cancers, such as CRTC2 [34], FBXL22 [35], OPRL1 [36], and PSMA4 [37]. Though the genes mentioned above mainly were differentially expressed between BCa and adjacent normal tissues (Supplementary Figure 2) and showed significant predictive values for prognosis (Supplementary Figures 3, 4), their functions in BCa have not been reported. Totally, the proposed model was helpful to identify novel biomarkers, providing cut-in points for further experimental researches.

However, the limitations of the present study should not be neglected. First, the research is retrospective, and a large-scale, multi-center, and prospective study was demanded to validate the clinical usefulness of CRRS. Second, some important phenotypes were associated

with the CRRS via bioinformatical analyses and big-data mining, and the experimental validation would be helpful.

In conclusion, a novel circadian rhythm-related signature was proposed, providing a useful tool to evaluate tumor immune infiltration, cisplatin efficacy, and prognosis in BCa.

MATERIALS AND METHODS

Data collection and processing

The transcriptome RNA sequencing data in count and FPKM format and corresponding clinical information were obtained from TCGA (https://portal.gdc.cancer.gov/) as the training dataset. GSE32894 dataset, which included the transcriptome data and clinicopathological features of 224 BCa cases, was directly downloaded from GEO (https://www.ncbi.nlm.nih.gov/geo/) as the external validation cohort. The Ensemble IDs and probe IDs were transformed into gene symbols according to the corresponding annotation files downloaded from the GENECODE (version 22, GRCh38) and GEO. The genes with average expression < 0.5 were excluded from the present study. The gene expression data with FPKM format and the prognosis information of 348 patients with metastatic urothelial carcinoma of IMvigor210 cohort were obtained from IMvigor210 CoreBiologies package in R (version 3.6.3). EdgeR package of R was used for genomic difference detection with $|logFC| > 1$ and adjusted $P < 0.05$ filtering. The volcano plot was drawn with the ggplot2 package to visualize the difference analysis.

Unsupervised clustering

The consensus clustering was conducted to identify the circadian subtypes of BCa through the ConsensusClusterPlus R package. We identified the optimal k value, equal to the clustering number, with the nmf R package. The slowest rising line in the cumulative distribution function (CDF) curve represented the best k value.

Survival analysis

To avoid including the deaths caused by surgical injury in the study, the cases with the following duration < 30 days were ruled out. The Kaplan-Meier survival analysis with log-rank test was performed with survival package of R. Survival R package was also used for univariate and multivariate Cox regression. Lasso was conducted by the glmnet R package, and 10-fold cross-validation was performed. The calibration plots were drawn with the rms package. The time-dependent ROC curves were completed with the survivalROC package.

Gene-pair strategy

Here, we utilized a gene-pair strategy to make the predictive model achieve broad applicability. We defined a novel combination of gene A and gene B, or A|B, as 1 when the expression value of A was higher than that of B; otherwise, it would be regarded as 0. The screened genes were cyclically paired, and a 0-or-1 matrix was successfully established after excluding the gene pairs with $< 20\%$ proportion of 0 or 1 in the training dataset.

Evaluation of immune infiltration

The ESTIMATE algorithm was used to evaluate the immune and stromal components ratios in TME, quantified as the Immune Score and Stromal Score [16]. The ESTIMATE Score represented the sum of the Immune Score and Stromal Score. The infiltration proportion of immune cells, including B cells, CD4 T cells, CD8 T cells, neutrophils, macrophages, and dendritic cells, were estimated on the TIMER website (http://cistrome.dfci.harvard.edu/TIMER/). The immunotherapeutic response was predicted with the TIDE algorithm, which offered an official website (http://tide.dfci.harvard.edu/).

The chemotherapeutic effectiveness analyses

The chemotherapeutic sensitivity of BCa patients in the TCGA-BLCA cohort was evaluated through the pRRophetic R package [38]. The transcriptome data and the IC50 values of 20 different BCa cell lines were retrieved from the GDSC database (https://www.cancerrxgene.org/) to confirm the predictive value of CRRS to chemotherapy response. The microarray RNA expression data from the GDSC dataset was normalized with Robust Multi-Array Average (RMA). The information about the response statuses to cisplatin among the BCa cases was also downloaded from TCGA, including complete response (CR), partial response (PR), clinical progressive disease (PD), and stable disease (SD).

GSEA and GSVA

The hallmark gene sets v. 7.2 was downloaded from MSigDB as the reference dataset. GSVA was conducted with the GSVA package of R, and the parameters were set as follows: min. size = 10, max. size =500, verbose = Ture, and parallel. size = 1. Limma was used for the difference detection, and the filtering threshold was set as $|logFC| > 0.1$ and adjusted $P < 0.05$. GSEA was

performed with GSEA software (version 4.1.0), and the number of permutations was set to 1000. The gene sets with nominal P < 0.05 and FDR q <0.05 were considered to be statistically significant.

Cell culture and treatment

The T24 cell line was purchased from Shanghai Institutes for Biological Sciences (Shanghai, China) and maintained in the McCoy's 5 A Medium (Gibco, USA) supplemented with 1% antibiotics and 10% fetal bovine serum (Gibco, USA). The cells were cultured in a humidified atmosphere with 5% CO_2 at 37° C. The cells were treated with 20μM cisplatin (Sigma-Aldrich, USA) for 24 hours.

RT-qPCR

The total RNA of the T24 cells were collected employing Trizol (ThermoFisher Scientific, Germany). Subsequently, PrimeScript RT Reagent Kit (Takara, China) and SYBR Premix ExTaq kit (Takara, China) were used to synthesize and amplify the cDNA. The ABI Prism 7000 system (Applied Biosystems, USA) helped identify the mRNA expression level, and the data were normalized with the 2-ΔΔC method.

Immunohistochemistry

The immunohistochemical staining of the CRRS genes was collected from The Human Protein Atlas (version 20.1; https://www.proteinatlas.org/), a comprehensive database for detecting the protein distribution and expression in human normal and tumor tissues.

The statistical analysis

We utilized R software (version 3.6.3) to conduct the statistical analysis. The student's t-test was utilized to compare the difference of the continuous variables obtained from vitro experiments. At the same time, the Wilcoxon Signed-rank test was adopted for the continuous variables collected from bioinformatical analyses. The violin diagrams and the boxplots were also drawn with the ggplot2 package. The Chi-square test was used for categorical variables, and the results were visualized with the ggplot2 and the ggstatsplot packages.

AUTHOR CONTRIBUTIONS

CDL designed the whole study and provided financial support. RRZ developed the algorithm, drew the plots, and conducted the vitro cell experiments. XYC and JJL wrote the original draft. QC, HT, and CY did help to editing and reviewing.

CONFLICTS OF INTEREST

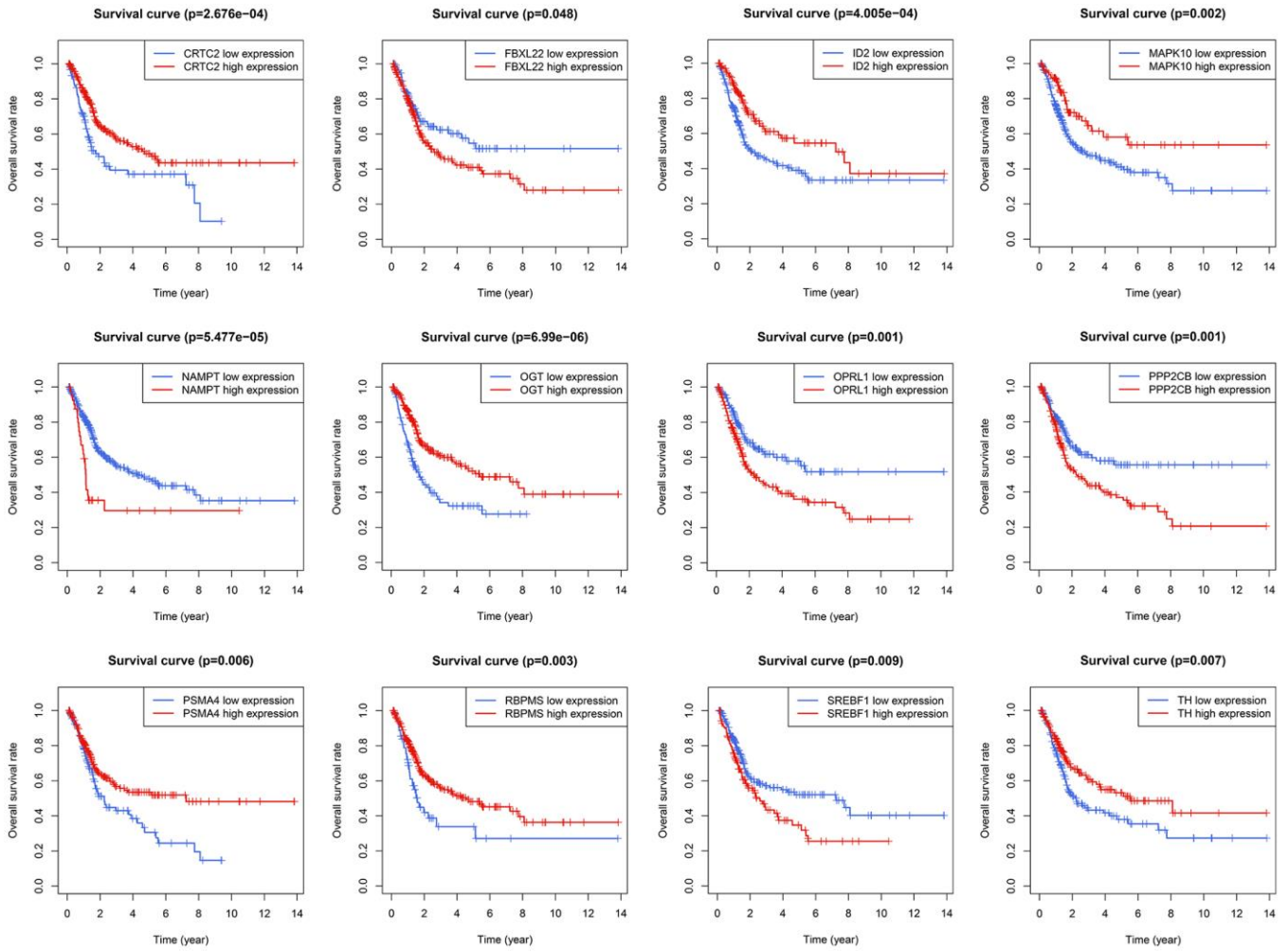The authors declared that they have no conflicts of interest.

REFERENCES

1. Patel VG, Oh WK, Galsky MD. Treatment of muscle-invasive and advanced bladder cancer in 2020. CA Cancer J Clin. 2020; 70:404–23.
   https://doi.org/10.3322/caac.21631 PMID:32767764

2. Lenis AT, Lec PM, Chamie K, Mshs MD. Bladder Cancer: A Review. JAMA. 2020; 324:1980–91.
   https://doi.org/10.1001/jama.2020.17598
   PMID:33201207

3. Tong H, Li T, Gao S, Yin H, Cao H, He W. An epithelial-mesenchymal transition-related long noncoding RNA signature correlates with the prognosis and progression in patients with bladder cancer. Biosci Rep. 2021; 41:BSR20203944.
   https://doi.org/10.1042/BSR20203944
   PMID:33289830

4. Wang J, Shen C, Dong D, Zhong X, Wang Y, Yang X. Identification and verification of an immune-related lncRNA signature for predicting the prognosis of patients with bladder cancer. Int Immunopharmacol. 2021; 90:107146.
   https://doi.org/10.1016/j.intimp.2020.107146
   PMID:33189610

5. Liu J, Ma H, Meng L, Liu X, Lv Z, Zhang Y, Wang J. Construction and External Validation of a Ferroptosis-Related Gene Signature of Predictive Value for the Overall Survival in Bladder Cancer. Front Mol Biosci. 2021; 8:675651.
   https://doi.org/10.3389/fmolb.2021.675651
   PMID:34095228

6. Sun X, Zhou Z, Zhang Y, Wang J, Zhao X, Jin L, Zhai T, Liu X, Zhang J, Mei W, Zhang B, Luo M, Yao X, Ye L. Identification and validation of a hypoxia-related prognostic and immune microenvironment signature in bladder cancer. Cancer Cell Int. 2021; 21:251.
   https://doi.org/10.1186/s12935-021-01954-4
   PMID:33962639

7. Sheng H, Zhang G, Huang Y, Sun L, Shi G, Ye D. A 5-lncRNA Signature Associated with Smoking Predicts the

Overall Survival of Patients with Muscle-Invasive Bladder Cancer. Dis Markers. 2021; 2021:8839747.
https://doi.org/10.1155/2021/8839747
PMID:33688381

8. Koronowski KB, Sassone-Corsi P. Communicating clocks shape circadian homeostasis. Science. 2021; 371:eabd0951.
https://doi.org/10.1126/science.abd0951
PMID:33574181

9. Hansen J. Night Shift Work and Risk of Breast Cancer. Curr Environ Health Rep. 2017; 4:325–39.
https://doi.org/10.1007/s40572-017-0155-y
PMID:28770538

10. Ruan W, Yuan X, Eltzschig HK. Circadian rhythm as a therapeutic target. Nat Rev Drug Discov. 2021; 20:287–307.
https://doi.org/10.1038/s41573-020-00109-w
PMID:33589815

11. Hassan SA, Ali AA, Yassine M, Sohn D, Pfeffer M, Jänicke RU, Korf HW, von Gall C. Relationship between locomotor activity rhythm and corticosterone levels during HCC development, progression, and treatment in a mouse model. J Pineal Res. 2021; 70:e12724.
https://doi.org/10.1111/jpi.12724 PMID:33615553

12. Li B, Cui Y, Diehn M, Li R. Development and Validation of an Individualized Immune Prognostic Signature in Early-Stage Nonsquamous Non-Small Cell Lung Cancer. JAMA Oncol. 2017; 3:1529–37.
https://doi.org/10.1001/jamaoncol.2017.1609
PMID:28687838

13. Hong W, Liang L, Gu Y, Qi Z, Qiu H, Yang X, Zeng W, Ma L, Xie J. Immune-Related lncRNA to Construct Novel Signature and Predict the Immune Landscape of Human Hepatocellular Carcinoma. Mol Ther Nucleic Acids. 2020; 22:937–47.
https://doi.org/10.1016/j.omtn.2020.10.002
PMID:33251044

14. Camp RL, Dolled-Filhart M, Rimm DL. X-tile: a new bio-informatics tool for biomarker assessment and outcome-based cut-point optimization. Clin Cancer Res. 2004; 10:7252–59.
https://doi.org/10.1158/1078-0432.CCR-04-0713
PMID:15534099

15. Zhang C, Zhang Z, Zhang G, Zhang Z, Luo Y, Wang F, Wang S, Che Y, Zeng Q, Sun N, He J. Clinical significance and inflammatory landscapes of a novel recurrence-associated immune signature in early-stage lung adenocarcinoma. Cancer Lett. 2020; 479:31–41.
https://doi.org/10.1016/j.canlet.2020.03.016
PMID:32201203

16. Yoshihara K, Shahmoradgoli M, Martínez E, Vegesna R, Kim H, Torres-Garcia W, Treviño V, Shen H, Laird PW, Levine DA, Carter SL, Getz G, Stemke-Hale K, et al. Inferring tumour purity and stromal and immune cell admixture from expression data. Nat Commun. 2013; 4:2612.
https://doi.org/10.1038/ncomms3612 PMID:24113773

17. Li T, Fu J, Zeng Z, Cohen D, Li J, Chen Q, Li B, Liu XS. TIMER2.0 for analysis of tumor-infiltrating immune cells. Nucleic Acids Res. 2020; 48:W509–14.
https://doi.org/10.1093/nar/gkaa407
PMID:32442275

18. Litchfield K, Reading JL, Puttick C, Thakkar K, Abbosh C, Bentham R, Watkins TB, Rosenthal R, Biswas D, Rowan A, Lim E, Al Bakir M, Turati V, et al. Meta-analysis of tumor- and T cell-intrinsic mechanisms of sensitization to checkpoint inhibition. Cell. 2021; 184:596–614.e14.
https://doi.org/10.1016/j.cell.2021.01.002
PMID:33508232

19. Jiang P, Gu S, Pan D, Fu J, Sahu A, Hu X, Li Z, Traugh N, Bu X, Li B, Liu J, Freeman GJ, Brown MA, et al. Signatures of T cell dysfunction and exclusion predict cancer immunotherapy response. Nat Med. 2018; 24:1550–58.
https://doi.org/10.1038/s41591-018-0136-1
PMID:30127393

20. Yang W, Soares J, Greninger P, Edelman EJ, Lightfoot H, Forbes S, Bindal N, Beare D, Smith JA, Thompson IR, Ramaswamy S, Futreal PA, Haber DA, et al. Genomics of Drug Sensitivity in Cancer (GDSC): a resource for therapeutic biomarker discovery in cancer cells. Nucleic Acids Res. 2013; 41:D955–61.
https://doi.org/10.1093/nar/gks1111
PMID:23180760

21. Yu M, Ozaki T, Sun D, Xing H, Wei B, An J, Yang J, Gao Y, Liu S, Kong C, Zhu Y. HIF-1α-dependent miR-424 induction confers cisplatin resistance on bladder cancer cells through down-regulation of pro-apoptotic UNC5B and SIRT4. J Exp Clin Cancer Res. 2020; 39:108.
https://doi.org/10.1186/s13046-020-01613-y
PMID:32522234

22. Shi T, Min M, Sun C, Zhang Y, Liang M, Sun Y. Does insomnia predict a high risk of cancer? A systematic review and meta-analysis of cohort studies. J Sleep Res. 2020; 29:e12876.
https://doi.org/10.1111/jsr.12876 PMID:31352687

23. Masri S, Sassone-Corsi P. The emerging link between cancer, metabolism, and circadian rhythms. Nat Med. 2018; 24:1795–803.
https://doi.org/10.1038/s41591-018-0271-8
PMID:30523327

24. Hastings MH, Reddy AB, Maywood ES. A clockwork web: circadian timing in brain and periphery, in health and disease. Nat Rev Neurosci. 2003; 4:649–61.

https://doi.org/10.1038/nrn1177
PMID:12894240

25. Garland SN, Irwin MR, Posner D, Perlis ML. Are sleep continuity disturbance and fatigue prodromal symptoms of cancer development? Med Hypotheses. 2018; 120:72–75.
https://doi.org/10.1016/j.mehy.2018.08.019
PMID:30220346

26. Xiang K, Xu Z, Hu YQ, He YS, Wu GC, Li TY, Wang XR, Ding LH, Zhang Q, Tao SS, Ye DQ, Pan HF, Wang DG. Circadian clock genes as promising therapeutic targets for autoimmune diseases. Autoimmun Rev. 2021; 20:102866.
https://doi.org/10.1016/j.autrev.2021.102866
PMID:34118460

27. Nathan P, Gibbs JE, Rainger GE, Chimen M. Changes in Circadian Rhythms Dysregulate Inflammation in Ageing: Focus on Leukocyte Trafficking. Front Immunol. 2021; 12:673405.
https://doi.org/10.3389/fimmu.2021.673405
PMID:34054857

28. Hadadi E, Acloque H. Role of circadian rhythm disorders on EMT and tumour-immune interactions in endocrine-related cancers. Endocr Relat Cancer. 2021; 28:R67–80.
https://doi.org/10.1530/ERC-20-0390 PMID:33446614

29. Wright KP Jr, Drake AL, Frey DJ, Fleshner M, Desouza CA, Gronfier C, Czeisler CA. Influence of sleep deprivation and circadian misalignment on cortisol, inflammatory markers, and cytokine balance. Brain Behav Immun. 2015; 47:24–34.
https://doi.org/10.1016/j.bbi.2015.01.004
PMID:25640603

30. Abreu M, Basti A, Genov N, Mazzoccoli G, Relógio A. The reciprocal interplay between TNFα and the circadian clock impacts on cell proliferation and migration in Hodgkin lymphoma cells. Sci Rep. 2018; 8:11474.
https://doi.org/10.1038/s41598-018-29847-z
PMID:30065253

31. Wang Z, Li F, Wei M, Zhang S, Wang T. Circadian Clock Protein PERIOD2 Suppresses the PI3K/Akt Pathway and Promotes Cisplatin Sensitivity in Ovarian Cancer. Cancer Manag Res. 2020; 12:11897–908.
https://doi.org/10.2147/CMAR.S278903
PMID:33244267

32. Liu SL, Lin HX, Lin CY, Sun XQ, Ye LP, Qiu F, Wen W, Hua X, Wu XQ, Li J, Song LB, Guo L. TIMELESS confers cisplatin resistance in nasopharyngeal carcinoma by activating the Wnt/β-catenin signaling pathway and promoting the epithelial mesenchymal transition. Cancer Lett. 2017; 402:117–30.
https://doi.org/10.1016/j.canlet.2017.05.022
PMID:28583847

33. Kang TH, Sancar A. Circadian regulation of DNA excision repair: implications for chrono-chemotherapy. Cell Cycle. 2009; 8:1665–67.
https://doi.org/10.4161/cc.8.11.8707
PMID:19411851

34. Fang M, Pak ML, Chamberlain L, Xing W, Yu H, Green MR. The CREB Coactivator CRTC2 Is a Lymphoma Tumor Suppressor that Preserves Genome Integrity through Transcription of DNA Mismatch Repair Genes. Cell Rep. 2015; 11:1350–57.
https://doi.org/10.1016/j.celrep.2015.04.052
PMID:26004186

35. Haddad SA, Ruiz-Narváez EA, Haiman CA, Sucheston-Campbell LE, Bensen JT, Zhu Q, Liu S, Yao S, Bandera EV, Rosenberg L, Olshan AF, Ambrosone CB, Palmer JR, Lunetta KL. An exome-wide analysis of low frequency and rare variants in relation to risk of breast cancer in African American Women: the AMBER Consortium. Carcinogenesis. 2016; 37:870–77.
https://doi.org/10.1093/carcin/bgw067
PMID:27267999

36. Lake SL, Jmor F, Dopierala J, Taktak AF, Coupland SE, Damato BE. Multiplex ligation-dependent probe amplification of conjunctival melanoma reveals common BRAF V600E gene mutation and gene copy number changes. Invest Ophthalmol Vis Sci. 2011; 52:5598–604.
https://doi.org/10.1167/iovs.10-6934
PMID:21693616

37. Wang T, Chen T, Thakur A, Liang Y, Gao L, Zhang S, Tian Y, Jin T, Liu JJ, Chen M. Association of PSMA4 polymorphisms with lung cancer susceptibility and response to cisplatin-based chemotherapy in a Chinese Han population. Clin Transl Oncol. 2015; 17:564–69.
https://doi.org/10.1007/s12094-015-1279-x
PMID:25744645

38. Geeleher P, Cox N, Huang RS. pRRophetic: an R package for prediction of clinical chemotherapeutic response from tumor gene expression levels. PLoS One. 2014; 9:e107468.
https://doi.org/10.1371/journal.pone.0107468
PMID:25229481

Supplementary Figure 1. The expression differences of the 16 CRRS genes between adjacent normal and BCa samples in the TCGA cohort (**A**) and GSE32894 cohort (**B**) via Wilcoxon signed-rank tests.
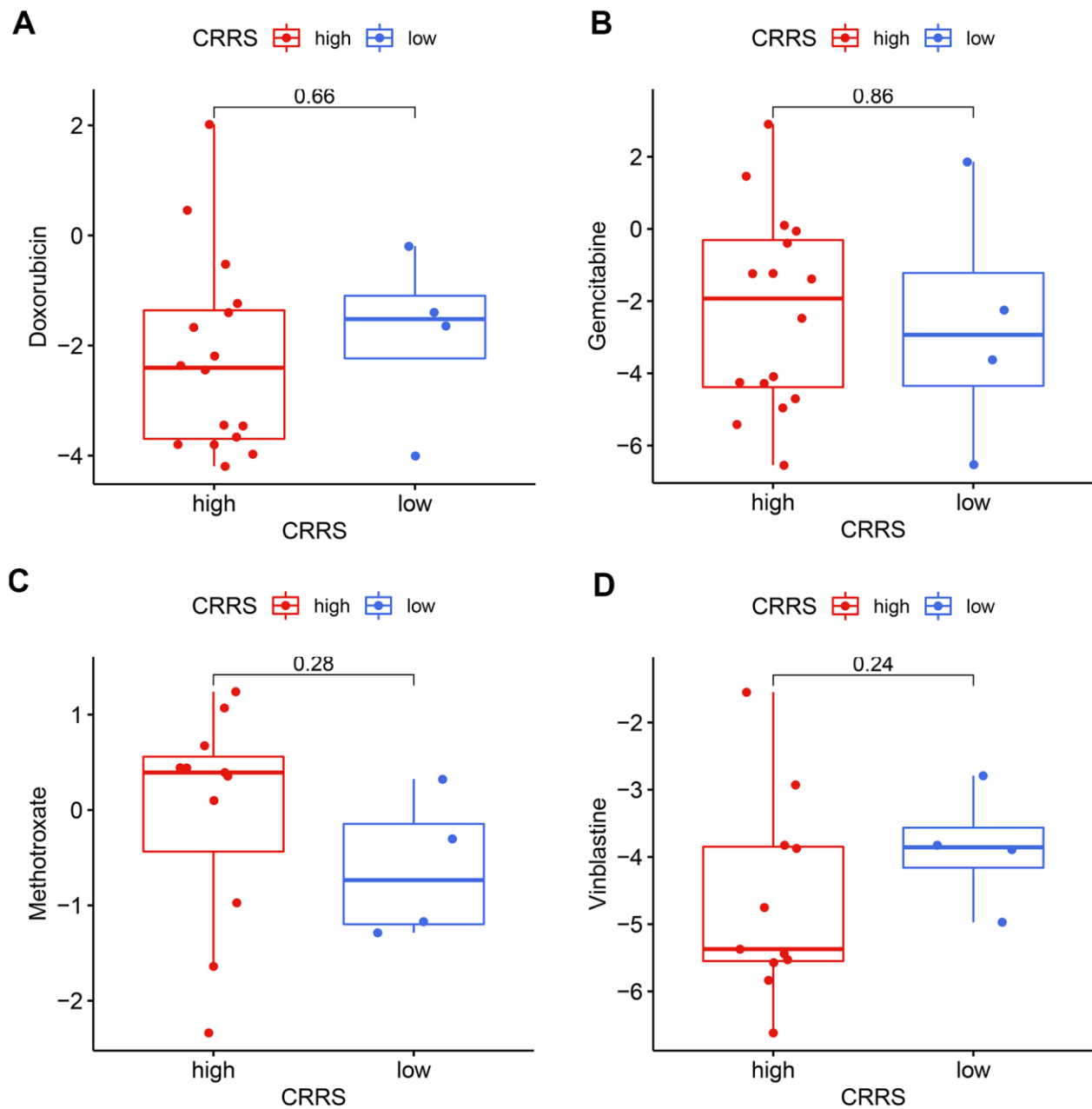
Supplementary Figure 2. The prognostic values of the 16 CRRS genes in the TCGA cohort.
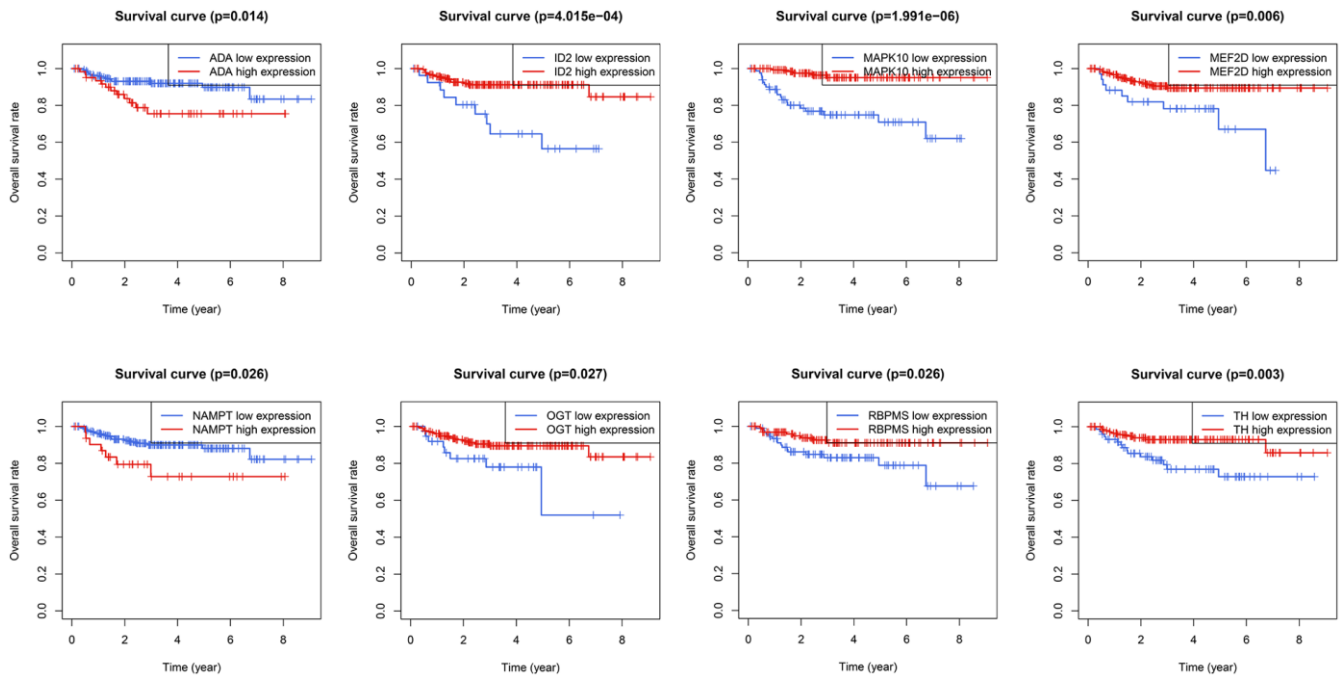
Supplementary Figure 3. The prognostic values of the 16 CRRS genes in the GSE32894 cohort.
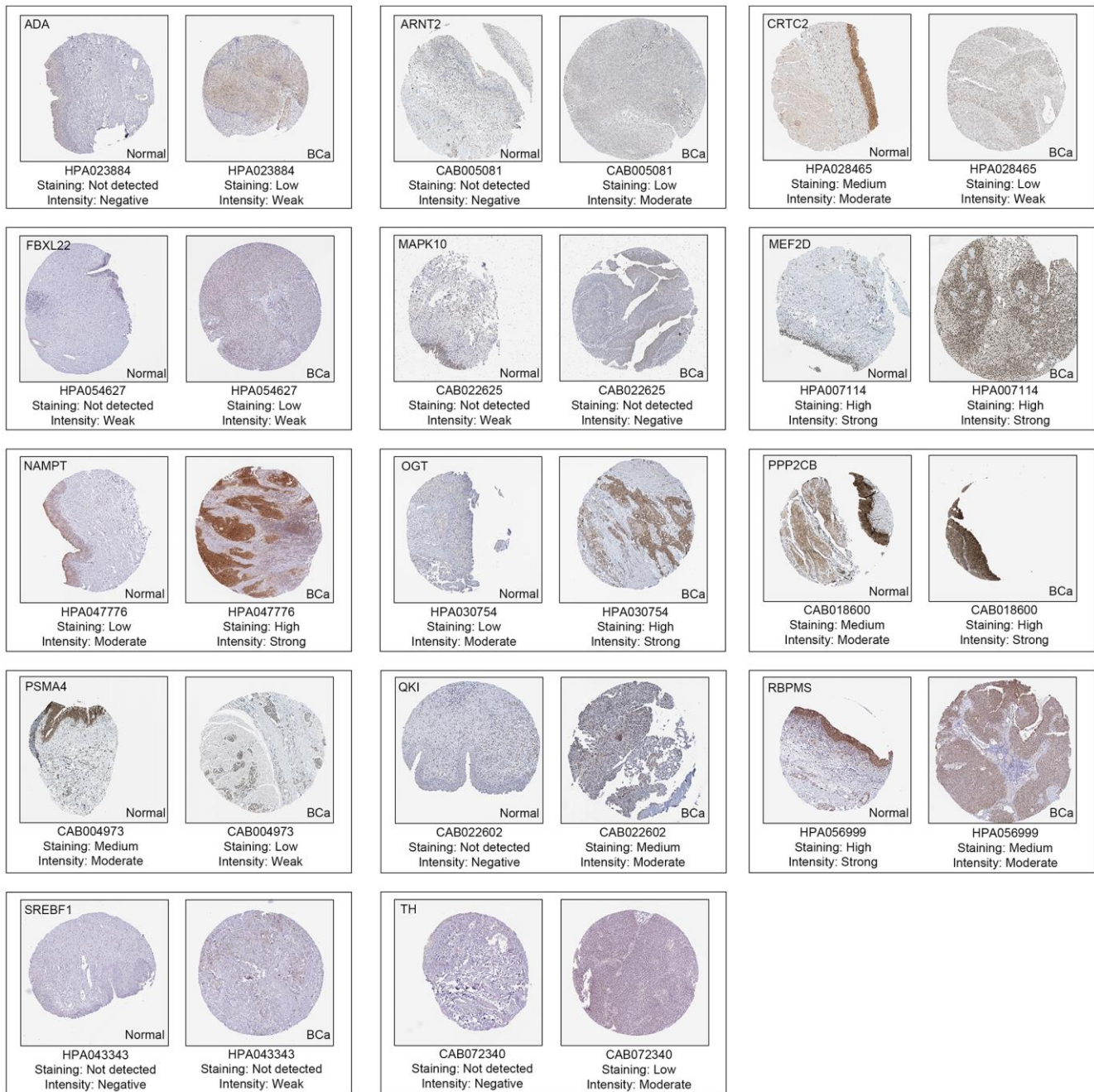
Supplementary Figure 4. The immunohistochemical staining of the CRRS genes in human normal and BCa tissues.

Supplementary Figure 5. The association between CRRS and the IC50 values of doxorubicin (**A**), gemcitabine (**B**), methotrexate (**C**), and vinblastine (**D**) in the BCa cell lines.

Supplementary Tables

Please browse Full Text version to see the data of Supplementary Tables 1–4, 7, 8, 11, 12, 15, 16

Supplementary Table 1. The circadian rhythm-related gene sets collected from MSigDB.

Supplementary Table 2. The circadian clustering of the 396 BCa cases from TCGA.

Supplementary Table 3. 122 circadian genes were differentially-expressed between adjacent normal and BCa samples.

Supplementary Table 4. The univariate Cox regression of 1667 gene pairs.

Supplementary Table 5. The details of the risk model by means of multivariate Cox regression with stepwise.

id	coef	HR	HR.95L	HR.95H	pvalue
PPP2CB|CRTC2	0.313859881	1.368697943	0.954190951	1.96326957	0.088156685
PSMA4|NAMPT	-0.546556531	0.578939944	0.393937839	0.850823215	0.005396217
QKI|RBPMS	0.329671729	1.390511589	0.972509447	1.988178609	0.070737473
ADA|MAPK10	0.316172646	1.371867083	0.882657423	2.132219412	0.15995725
ARNT2|OPRL1	-0.687965343	0.502597643	0.363026562	0.695828948	0.000034
ID2|SREBF1	-0.437329062	0.645758902	0.455211219	0.916068282	0.014232299
OGT|MEF2D	-0.558600847	0.572008832	0.40672795	0.804454437	0.001324701
TH|FBXL22	-0.350313151	0.704467451	0.493085274	1.006467675	0.054286136

Supplementary Table 6. The spearman correlation coefficients between the 16 CRRS genes and circadian transcription factors.

TF	CRRS_gene	Spearman_correlation	pvalue
PER1	PPP2CB	0.282	5.78093075573597E-09
PER1	PSMA4	-0.065	0.189990010775076
PER1	QKI	0.219	0.0000073556873937004
PER1	ADA	0.209	0.0000186748072864482
PER1	ARNT2	-0.08	0.107097529553661
PER1	ID2	-0.018	0.721606561422284
PER1	OGT	-0.156	0.00151541828986829
PER1	TH	-0.262	6.9347012076925E-08
PER1	CRTC2	-0.005	0.922923590920486
PER1	NAMPT	0.277	1.19788307528409E-08
PER1	RBPMS	0.014	0.77648121597283
PER1	MAPK10	-0.162	0.0010125040968491
PER1	OPRL1	0.096	0.052485601947928
PER1	SREBF1	-0.07	0.156794917100766
PER1	MEF2D	0.48	4.98238207011712E-25
PER1	FBXL22	0.097	0.048404465245423
ARNTL	PPP2CB	0.286	3.64444944036374E-09
ARNTL	PSMA4	0.054	0.274365487857749
ARNTL	QKI	0.312	9.23587578673394E-11
ARNTL	ADA	0.304	3.32072102294723E-10
ARNTL	ARNT2	0.014	0.7774721796168
ARNTL	ID2	-0.176	0.000345442760082285
ARNTL	OGT	0.042	0.400897836235977
ARNTL	TH	-0.262	6.79031747327374E-08
ARNTL	CRTC2	-0.06	0.221922108953692
ARNTL	NAMPT	0.345	5.98192804606054E-13
ARNTL	RBPMS	-0.187	0.000142868750526303
ARNTL	MAPK10	-0.114	0.0212632782405979
ARNTL	OPRL1	0.183	0.000193893613183833
ARNTL	SREBF1	-0.047	0.337795375026129
ARNTL	MEF2D	0.297	8.00068086478635E-10
ARNTL	FBXL22	-0.085	0.0834569272544813
CLOCK	PPP2CB	0.323	1.98215465907806E-11
CLOCK	PSMA4	-0.005	0.914261633994987
CLOCK	QKI	0.317	4.82035133174775E-11
CLOCK	ADA	-0.045	0.366248093309971
CLOCK	ARNT2	0.166	0.000732603609458834
CLOCK	ID2	-0.033	0.49877762642488
CLOCK	OGT	0.113	0.0221696188543565
CLOCK	TH	-0.047	0.341038087379232
CLOCK	CRTC2	-0.074	0.135200126646786
CLOCK	NAMPT	0.396	6.93387354272534E-17
CLOCK	RBPMS	-0.101	0.0415707788595762
CLOCK	MAPK10	0.184	0.000171536398851449
CLOCK	OPRL1	-0.042	0.394053495180797
CLOCK	SREBF1	0.096	0.0519505258236541
CLOCK	MEF2D	0.203	0.0000352825690784988

CLOCK	FBXL22	-0.102	0.0393201635250358
PER2	PPP2CB	0.364	2.76579194910235E-14
PER2	PSMA4	-0.13	0.00819041404470939
PER2	QKI	0.196	0.0000624473549864017
PER2	ADA	-0.004	0.928426331367054
PER2	ARNT2	0.064	0.195850407221862
PER2	ID2	0.024	0.622194590931014
PER2	OGT	0.065	0.190822565288749
PER2	TH	-0.21	0.0000172810300478247
PER2	CRTC2	-0.194	0.0000736024601316075
PER2	NAMPT	0.386	4.68094755849204E-16
PER2	RBPMS	0.076	0.126229351152509
PER2	MAPK10	0.156	0.00147065559316406
PER2	OPRL1	-0.058	0.237002835558395
PER2	SREBF1	0.026	0.603929368408065
PER2	MEF2D	0.29	2.22340540332294E-09
PER2	FBXL22	-0.013	0.787736262994609

Supplementary Table 7. The evaluated CRRS and risk stratification of the patients from TCGA.

Supplementary Table 8. The evaluated CRRS and risk stratification of the patients from GSE32894.

Supplementary Table 9. The P values of the 16 CRRS genes via Kaplan-Meier survival analysis in the TCGA cohort.

Gene	pvalue
PPP2CB	0.00119351373210486
PSMA4	0.00553335180691217
QKI	0.0531965137366481
ADA	0.145667391494244
ARNT2	0.0875637046442688
ID2	0.000400456719568121
OGT	6.99019535410628E-06
TH	0.00739078078934785
CRTC2	0.000267642081746122
NAMPT	0.0000547669235902992
RBPMS	0.00278692797305302
MAPK10	0.00170324171058989
OPRL1	0.00100260158060006
SREBF1	0.00886033858742974
MEF2D	0.0836396104281839
FBXL22	0.0484398887539246

Supplementary Table 10. The P values of the 16 CRRS genes via Kaplan-Meier survival analysis in the GSE32894 cohort.

Gene	pvalue
PPP2CB	0.19840575657814
PSMA4	0.0512927853392764
QKI	0.0737557610829734
ADA	0.0137360739475768
ARNT2	0.212478890791293
ID2	0.000401526258070994
OGT	0.0268431273486096
TH	0.00336694319562603
CRTC2	0.448685428580084
NAMPT	0.026193748611878
RBPMS	0.0263911073223753
MAPK10	1.99072940310074E-06
OPRL1	0.060364305328372
SREBF1	0.128023643497365
MEF2D	0.00565422501840018
FBXL22	0.625931543379857

Supplementary Table 11. The GSVA scores of the 7 gene clusters representing different immune and inflammatory responses.

Supplementary Table 12. The calculated CRRS of IMvigor210 cohort.

Supplementary Table 13. The IC50 values and calculated CRRS of the 20 BCa cell lines.

id	CRRS	Risk	Cisplatin	Methotrexate	Doxorubicin	Vinblastine	Gemcitabine
SW780	0.6218074	high	2.5401121	-2.33514264	2.0186005	-5.834158	2.90442625
5637	0.5583428	high	1.5233729	-1.63878302	-3.7970998	-6.615991	-1.2320148
T_24	0.8646304	high	NA	NA	-1.2347614	NA	-0.05737397
KU_19_19	0.4345612	high	2.1894818	-0.971251	0.4585119	-3.870262	1.46146064
HT_1197	0.4345612	high	3.5162574	0.44139082	-1.4008072	-1.548121	-0.39201549
CAL_29	0.4015377	high	2.1125156	0.3566166	-2.1881597	-5.527362	-4.09075495
VM_CUB_1	0.8646304	high	NA	NA	-2.4430689	NA	-4.27746705
BFTC_905	0.4345612	high	1.0370687	0.09939585	-4.19149	-5.570882	-6.54221767
TCCSUP	0.4345612	high	NA	NA	-0.5197181	NA	0.10590606
UM_UC_3	0.8646304	high	1.7794393	0.67527913	-2.3634623	-4.751309	-4.24944117
J82	0.8646304	high	NA	NA	-3.6614741	NA	-4.70299634
RT_112	0.4015377	high	NA	NA	-3.795467	NA	-5.41436675
SCaBER	0.8646304	high	2.484372	1.07195731	-3.4567252	-5.439199	-2.47287178
647_V	0.8646304	high	2.2538245	0.3929999	-3.4446805	-3.825809	-4.9542453
639_V	0.8646304	high	0.7969217	0.44358272	-3.9721519	-5.371709	-1.38215512
HT_1376	0.3167663	high	NA	1.23989051	-1.6657156	-2.927075	-1.2352954
DSH1	0.3124189	low	3.8393146	-1.28696771	-1.6432175	-3.823059	-2.24507309
SW1710	0.2018119	low	3.4772703	0.32408962	-4.004044	-4.970615	-6.5276792
RT4	0.1471075	low	2.7182992	-1.16844661	-0.1939384	-2.791072	1.86036582
LB831_BLC	0.2806218	low	4.0320381	-0.30205164	-1.3963335	-3.890481	-3.62147262

Supplementary Table 14. The sequence of the primers used in the present study.

Gene symbol	ForwardPrimer(5'->3')	ReversePrimer(5'->3')
GAPDH	GGAGCGAGATCCCTCCAAAAT	GGCTGTTGTCATACTTCTCATGG
PPP2CB	CTGAACGAGAACCAAGTGCG	ACGAACCTCTTGCACATTTGA
PSMA4	AGTGTGGCAGGCATAACTTCT	TCACAAGGTATTGGCTCCTGA
QKI	AAGCCCACCCCAGATTACCT	ACTCTGCTAATTTCTTCGTCCAG
ADA	GCCTTCGACAAGCCCAAAGTA	CTCTGCTGTGTTAGCTGGGAG
ARNT2	ATGGCGCGTACAAGCCTTC	AGTCAGACACATAAATCACTCGC
ID2	AGTCCCGTGAGGTCCGTTAG	AGTCGTTCATGTTGTATAGCAGG
OGT	TCCTGATTTGTACTGTGTTCGC	AAGCTACTGCAAAGTTCGGTT
TH	GGAAGGCCGTGCTAAACCT	GGATTTTGGCTTCAAACGTCTC
CRTC2	CCGGTTACAGGCCCAAAAACT	AATGTGGCGGGTGTATCGG
NAMPT	CGGCAGAAGCCGAGTTCAA	GCTTGTGTTGGGTGGATATTGTT
RBPMS	AAACAGCCTGTAGGTTTTGTCA	GGAATTTCAGGATCGAAGCGG
MAPK10	CAGATGGAATTAGACCATGAGCG	TCAATGTGCAATCAGACTTGACT
OPRL1	TTCTGGGAGGTTATCTACGGC	GGATGACGTACATGACAAGGC
SREBF1	ACAGTGACTTCCCTGGCCTAT	GCATGGACGGGTACATCTTCAA
MEF2D	CCAGCGAATCACCGACGAG	GCAGTCACATAGCACGCTC
FBXL22	CCATGCACATAACCCAGCTCA	CCGAGGTGATTTCGGTCCAAC

Supplementary Table 15. The differential analysis of the phenotypes via limma package.

Supplementary Table 16. The GSEA results in the subgroup with high CRRS.

Supplementary Table 17. The GSEA results in the subgroup with low CRRS.

NAME	GS follow link to MSigDB	GS DETAILS	SIZE	ES	NES	NOM p-val	FDR q-val	FWER p-val	RANK AT MAX	LEADING EDGE
HALLMARK_ OXIDATIVE_ PHOSPHORYLATION	HALLMARK_ OXIDATIVE_ PHOSPHORYLATION	Details ...	185	-0.32739022	-1.4821173	0.004026846	0.0662548	0.288	3605	tags=27%, list=18%, signal=33%
HALLMARK_ BILE_ACID_ METABOLISM	HALLMARK_ BILE_ACID_ METABOLISM	Details ...	112	-0.29618245	-1.2587848	0.09154929	0.29479158	0.937	4446	tags=33%, list=23%, signal=43%
HALLMARK_ PEROXISOME	HALLMARK_ PEROXISOME	Details ...	104	-0.29905438	-1.2510827	0.10557185	0.20794153	0.95	4667	tags=33%, list=24%, signal=43%
HALLMARK_ DNA_REPAIR	HALLMARK_ DNA_REPAIR	Details ...	148	-0.26814818	-1.1834313	0.15096954	0.2667444	0.994	5692	tags=38%, list=29%, signal=53%
HALLMARK_ FATTY_ACID_ METABOLISM	HALLMARK_ FATTY_ACID_ METABOLISM	Details ...	156	-0.26005426	-1.1436396	0.2021858	0.28168854	0.998	2758	tags=21%, list=14%, signal=24%
HALLMARK_ ADIPOGENESIS	HALLMARK_ ADIPOGENESIS	Details ...	197	-0.2361732	-1.0680834	0.30717185	0.3783189	1	2588	tags=19%, list=13%, signal=22%
HALLMARK_ SPERMATOGENESIS	HALLMARK_ SPERMATOGENESIS	Details ...	132	-0.14034766	-0.61015123	0.9958506	0.9962178	1	5174	tags=23%, list=26%, signal=31%